FACULDADE DE MEDICINA DA UNIVERSIDADE DE COIMBRA

TRABALHO FINAL DO 6º ANO MÉDICO COM VISTA À ATRIBUIÇÃO DO GRAU DE MESTRE NO ÂMBITO DO CICLO DE ESTUDOS DE MESTRADO INTEGRADO EM MEDICINA

CÁTIA MARISA ALVES FERREIRA

GENOTYPHE-PHENOTYPE CORRELATIONS IN BEST1 ASSOCIATED DISEASES

ARTIGO CIENTÍFICO

ÁREA CIENTÍFICA DE OFTALMOLOGIA

TRABALHO REALIZADO SOB A ORIENTAÇÃO DE:
PROF. DOUTOR EDUARDO JOSÉ GIL DUARTE SILVA

MARÇO/2010

Index

Abbreviations

BVMD – Best Vitelliform Macular Dystrophy

ARB – Autosomal Recessive Bestrophinopathy

CNV – Choroidal Neovascularization

BCVA – Best corrected visual acuity

dHPLC – denaturing high-performance liquid chromatography

EOG – Electro-oculogram

mfERG – multifocal Electroretinography

OCT – Optical Coherence Tomography

RPE – retinal pigment epithelium

ISCEV – International Society for Clinical Electrophysiology of Vision

Abstract

Purpose: to evaluate genotype-phenotype correlations in the *BEST1* mutation spectrum and check whether the Portuguese findings fit the continuum observed in other populations.

Methods: twenty four affected individuals and thirteen controls from eleven unrelated families (twenty four males, thirteen females, ages between 10 and 59 years) were characterized by mutation analysis with a combination of denaturing high-performance liquid chromatography (dHPLC) and direct sequencing, and clinical examination. Electrophysiology (EOG and mfERG) and optical coherence tomography (OCT) were additionally performed whenever possible.

Results: We identified four novel *BEST1* mutations in four unrelated families (three in patients with Best disease and one in ARB patients). In BVMD patients, we found 3 causative sequence changes in *BEST1* gene. Two families with BVMD and a case of multifocal Best had no mutations in *BEST1*. According to mfERG measurements there is a significant peripheral impairment of retinal function in BVMD. Furthermore, changes in thickness of the neurosensory retina, as measured by OCT, and reduced mfERG responses were also indicators of early loss in BVMD and often occurred even with preserved visual acuity. There was a substantial reduction in mfERG amplitude responses in BVMD and ARB patients.

Conclusions: Several novel *BEST1* mutations were found and genotype-phenotype correlations were addressed. EOG was abnormal or subnormal in almost all patients even when visual acuity is unaltered. ARB patients showed lower Arden ratio on EOG than BVMD ones. The lesion area did not depend on the mutation and did not correlate with visual

acuity. Generally, lower visual acuity was associated with advanced BVMD stages, mostly with the atrophic stage. Disease duration does not correlate with mfERG measurements.

Resumo

Objectivo: avaliar correlações genótipo-fenótipo no espectro de mutações do gene *BEST1* e determinar se os achados na população portuguesa são concordantes com o observado noutras populações.

Métodos: Foram caracterizados vinte e quatro indivíduos afectados e treze normais, pertencentes a onze famílias diferentes (vinte e quatro do sexo masculino e treze do sexo feminino, com idades compreendidas entre 10 e 59 anos). Foi realizada uma avaliação clínica e molecular, através da análise de mutações com dHPLC e por sequenciação directa. A análise fenotípica incluiu a realização de testes anatomo-funcionais, incluindo electro-oculograma (EOG), electroretinograma multifocal (mfERG) e tomografia de coerência óptica (OCT).

Resultados: Foram identificadas quatro mutações novas em quatro famílias independentes (três com doença de Best e uma com bestrofinopatia autossómica recessiva). Em duas das famílias com doença de Best e num caso de Best multifocal não foram identificadas mutações no gene *BEST1*. De acordo com os dados do ERG multifocal, existe um aumento significativo da função retiniana periférica nos doentes com BVMD. Outros indicadores de lesão precoce na doença de Best são as alterações na espessura da retina neurosensorial, medida através de OCT, e a diminuição das respostas no ERG multifocal. Estas alterações podem estar presentes mesmo quando a acuidade visual está preservada.

Existe uma diminuição significativa da amplitude das respostas tanto nos doentes com BVMD como nos doentes com ARB.

Conclusões: Foram identificadas novas mutações que permitem inferir correlações genótipo-fenótipo. O EOG revela-se anormal ou subnormal na maioria dos doentes, mesmo quando a acuidade visual é normal. Os doentes com ARB apresentam índices de Arden mais baixos do que os doentes com BVMD. A área da lesão não está relacionada com a mutação subjacente nem com a acuidade visual. Em regra, uma acuidade visual baixa está associada a estadios mais avançados da doença, principalmente ao estadio atrófico. A duração da doença não está relacionada com o grau de alterações no ERG multifocal.

Keywords Best Vitelliform Macular Dystrophy · Autosomal Recessive Bestrophinopathy · multifocal Best · retinal pigmented epithelium · *BEST1* gene · Arden ratio · multifocal electroretinogram · optical coherence tomography

Introduction

Best Disease or Best Vitelliform Macular Dystrophy (BVMD) is an autosomal dominant (AD) disorder, with incomplete penetrance and variable phenotypic expressivity (Boon et al., 2009). It is one of the most common retinal dystrophies and it predominantly affects the macula (Boon et al., 2009).

BVMD was first described in 1905 by Friedrich Best, a German Ophthalmologist. This macular dystrophy usually begins during the first or second decade of life, but it is highly variable, with mean in the fourth decade (Mohler and Fine, 1981; Seddon et al., 2003; Wabbels et al., 2006). Most cases show a solitary lesion in the macula (unifocal), others have multifocal lesions that confine to the posterior pole (Querques et al., 2008).

Decreased visual acuity may be the first symptom describe by BVMD patients. Other symptoms are metamorphopsia, photophobia, and loss of night vision. Mild to marked hypermetropia is a common associated finding (Boon et al., 2009). It was shown that there is a high correlation between patient age and visual acuity (Fishman et al, 1993; Boon et al., 2009).

Many classifications have been proposed, based on ophthalmoscopic aspect of the lesions. Friedrich Best classification proposes five stages: *previtelliform stage*, in which the fovea is normal or shows discrete RPE alterations; *vitelliform stage*, with a well circumscribed macular lesion, completely filled by yellowish material, resembling an egg yolk; *pseudohypopyon stage*, with yellow material accumulated inferiorly; *vitelliruptive stage*, in which the previously confluent vitelliform material breaks up; and the *atrophic*

stage, with final chorioretinal atrophy (Querques et al., 2008). Gass, in 1997, also described a sixth stage: *cicatricial stage* and/or *neovascular stage*, in which subsequent scarring appears due to choroidal neovascularization (Boon et al., 2009). Some BVMD patients can show a different stage in each eye and many lesions simultaneously show characteristics of different BVMD stages (Boon et al., 2009). Even in the sixth stage, despite central starring, patients often retain a good visual acuity (Chung et al., 2001).

Choroidal neovascularization (CNV) is often difficult to recognize in BVMD lesions, but it occurs in 2-9% of cases (Chung et al., 2001; Boon et al., 2009). The presence of CNV may be inferred when there is subretinal hemorrhage or a grayish-green scar within a lesion (Chung et al., 2001; Boon et al., 2009). CNV in BVMD lesions often occurs after ocular trauma, according to some reports (Chung et al., 2001; Boon et al., 2009).

BVMD was the first disease reported to have a cause-effect correlation with mutations in the *BEST1 gene* (Petrukhin et al., 1998). The *BEST1 gene* maps to chromosome 11q12-q13; it is mainly expressed in the retinal pigmented epithelium (RPE) but also in kidney, spinal cord, brain and testis (Boon et al., 2009; Petrukhin et al., 1998). *BEST1 gene* encodes the *bestrophin-1 protein*, which is located in the basolateral plasma membrane of the RPE. It may also be found in the intracellular space (Boon et al., 2009). This protein is involved in the transport of Ca^{2+}/Cl^{-} through the basolateral plasma membrane of RPE and also modulates activity of voltage gated L-type Ca^{2+} channels (Wabbels et al., 2006). The normal function of this channel depends upon appropriate bestrophin oligomerisation, thus mutations in the *BEST1* gene will lead to various extent of disease severity and may affect penetrance (Wabbels et al., 2006).

Posterior studies also found *BEST1 gene* mutations in patients with Adult-onset Foveomacular Vitelliform Dystrophy (AFVD). In addition, *BEST1* mutations can also cause ADVIRC (AD Vitreoretinochoroidopathy), ADMRCS Syndrome (Microcornea, rod-cone dystrophy, early-onset cataract and posterior staphyloma) and ARB (Autosomal Recessive Bestrophynopathy) (Boon et al., 2009; Burgess et al., 2008).

Autosomal recessive bestrophinopathy (ARB) is a distinct retinal disorder that results from biallelic mutations in *BEST1*. It is associated with central visual loss, a characteristic retinopathy, absent electro-oculogram light rise and a reduced electroretinogram. Heterozygote patients have no clinical or electrophysiological abnormalities (Burgess et al., 2008).

The aims of this paper are to clinically and genetically characterize eleven independent Portuguese families carrying the diagnosis of either BVMD or ARB, to perform a complete clinical evaluation which includes structural (OCT), and electrophysiological (multifocal ERG and EOG) studies of all affected individuals and their relatives. Molecular genetics of these cases were performed elsewhere as a part of an international collaboration. We also propose to evaluate possible genotype-phenotype correlations in the *BEST1* mutation spectrum, and check whether the Portuguese findings fit the continuum observed in other populations.

Materials and Methods

Patient and control population

Thirty seven individuals from eleven unrelated families (twenty four males, thirteen females, ages between 10 and 59 years) were included in this study. Twenty four are affected, and thirteen are healthy controls. All affected individuals are followed at the Centre for Hereditary Eye Diseases of the Department of Ophthalmology, University Hospital of Coimbra. Probands and affected family members presented at our clinic mostly due to visual impairment (loss of central vision) or funduscopic changes that fit the clinical diagnosis of Best disease, autosomal recessive bestrophinopathy, or multifocal Best.

All individuals included in the study were informed about its objectives and volunteered to participate. Informed consent was obtained from all subjects according to the tenets of the declaration of Helsinki. The study was approved by the Ethics Committee of the University Hospital of Coimbra.

Clinical Examination

Ophthalmic examination included assessment of best corrected visual acuity (BCVA) after manifest or cycloplegic refraction, slit-lamp examination and fundus examination using a non-contact 78-diopter lens. Fundus photography was performed with a TOPCON TRC 50X (Topcon Optical, Tokyo, Japan).

Electrophysiology (EOG and ERG)

Electrooculograms (EOG) were recorded in all patients according to the ISCEV-standard using a Nicolet Spirit-System (Nicolet Biomed, USA). According to our normative database Arden ratios were rated pathologic below 1.80. Eye movements were monitored during recording and the original waveforms were displayed. The amplitude of collection was automatically measured by the system and plotted. This was checked for plausibility.

Multifocal ERGs (mfERGs) were recorded using DTL fiber electrodes, after a light adaptation period of 10 minutes and pupil dilation with tropicamide, before fundus photography, with a commercial system (RETIscan System; Roland Consult) (Kutschbach, 1997). Refractive errors were corrected in relation to the viewing distance. The stimulus used in the mfERG consisted of 61 hexagons covering a visual field of up to 30° and presented on a 20-inch monitor at a viewing distance of 33 cm. Luminance was 120 cd/m2 for white hexagons and approximately 1 cd/m2 for black hexagons, resulting in a Michelson contrast of 99%. The hexagonal areas increased with eccentricity to compensate for local differences in signal amplitude because of differences in cone density across the retina (leading to a fourfold change in hexagon area size). Each hexagon was temporally modulated between light and dark according to a binary m-sequence (frame rate, 60 Hz). Observers were instructed to fixate a small black cross in the center of the stimulus. Fixation was continuously checked by means of online video-monitoring during the approximately 8-minute recording sessions. To improve fixation stability, sessions were broken into 47-second segments; eight trials were recorded in total. Signals were amplified with a gain of 100,000 and were band-pass filtered (5–300 Hz).

Reference and ground electrodes were attached to the ipsilateral outer canthus and forehead, respectively. The surface electrode impedance was less than 10 k_. Analyses were performed with the system software (RETIscan; Roland Consult) and standard statistical packages. First-order kernels were used for mfERG analysis because of their close correlation with the function of the outer retina (Hood, 1997). The obtained local ERGs responses were normalized by the area of stimulus delivery to obtain a density response (nV/deg^2). For each hexagon, the peak amplitude of P1—defined as the difference between N1 and P1 amplitudes—the N1 peak, and the implicit time of P1 component were computed. To easily evaluate spatial differences of the local ERG responses, responses from the 61 elements were divided into averages of five concentric rings around the fovea.

Optical Coherence Tomography (OCT)

OCT was performed with commercially available equipment in fourteen BVMD patients, three ARB patients and two with multifocal Best. We used an OCT device (Stratus OCT; Carl Zeiss Meditec, Dublin, CA) to obtain cross-sectional images centered in the macula,26 with axial resolution of 10 _m or less, transversal resolution of 20 _m, and longitudinal scan range of 2 mm. With this OCT device (Stratus OCT; Carl Zeiss Meditec), six radial line scans 6 mm in length and 128 A-scans 30° apart were scanned in 1.92 seconds, and a nine-region retinal thickness map was obtained by segmenting the retina from other layers with an algorithm detecting the edge of the RPE and the photoreceptor layer.

Macular retinal thickness was calculated by computing the distance between the signal from the vitreoretinal interface and the signal from the anterior boundary of the RPE. Retinal thickness was presented as a nine-region thickness map showing the interpolated

thickness for each area, with a central circle of 500 _m radius (ring 0) and two outer circles with radii of 1500 _m (ring 1) and 3000 _m (ring 2). The interpolated thickness was displayed using a false color scale, in which bright colors (red and white) corresponded to thickened areas and darker colors (blue and black) were assigned to thinner areas.

Molecular genetic analysis

Genomic DNA was extracted using an automated DNA extractor (BioRobot EZ1, Qiagen, Hilden, Germany). The 11 exons of gene *BEST1* were PCR-amplified using previously described primers and conditions (Petrukhin et al., 1998). To detect sequence changes, all exons of *BEST1* were screened by dHPLC using a WAVE ^{TM} DNA Fragment Analysis System (Transgenomic). The PCR amplicons from control DNA and test DNA were combined in 1:1 ratio and were loaded (5µl) on a C_{18} reserved-phase column (DNA Sep^{TM} column; Transgenomic). The column mobile phase consisted of an acetonitrile gradient formed by mixing buffers A and B (WAVE Optimized^{TM}; Transgenomic). The flow rate was set at 0.9 ml/min and DNA was detected at 260 nm. For each amplicon, three optimum temperatures for hetero- and homodimer detection were determined empirically. The chromatograms obtained with the control and test samples were compared for the peak number and shape, for each temperature. All abnormal heteroduplexes obtained were, then, sequenced. Amplification products were purified with QIA-quick Gel Extraction Kit (Qiagen). Sequencing reactions were performed using the 4-dye terminator cycle sequencing ready reaction kit (BigDye DNA Sequencing Kit, Applied Biosystems, Foster City, CA). Sequence products were purified through fine columns (Sephadex G-501, Princetown Separations, Adelphia, NJ) and resolved in an ABI Prism 3130 (Applied Biosystems). In those cases, in which no mutation

was detected using dHPLC screening, all *BEST1* exons were directly sequenced to guarantee that all sequence changes were identified.

Results

Clinical and molecular findings

The individual clinical details are summarized in **Table I** (BVMD patients), **II** (ARB patients) and **III** (multifocal Best patients) and the pedigrees are shown in **Figure 1 – 7**. Representative images from fundus photography of BVMD and ARB patients are shown in **Figure 8** and **9.**

We identified the causative *BEST1* mutations in 4 families of the 11 tested families (3 BVMD families and 1 ARB family). All mutations are summarized in **Tables I** and **II**, respectively. All were novel missense mutations located in exons 2 and 6. The novel sequence changes were classified as disease-causing based on the following criteria: segregation within the family, location within regions known to be frequently affected by mutations ('hotspot' regions) and degree of conservation in the bestrophin-related family members. For consistency, we used the homologies suggested by Marquardt and colleagues (Marquardt et al., 1998) for multiple sequence alignment of predicted human *BEST1* with putative proteins from *C..elegans* of 47.7 (P34577), 73.8 (P34672) and 47.8 kDa (Q09379) as well as the partial EST-encoded sequences from *D. melanogaster* (AA817295), *Mus musculus* (AA497726) and human (AA621745, AA777061).

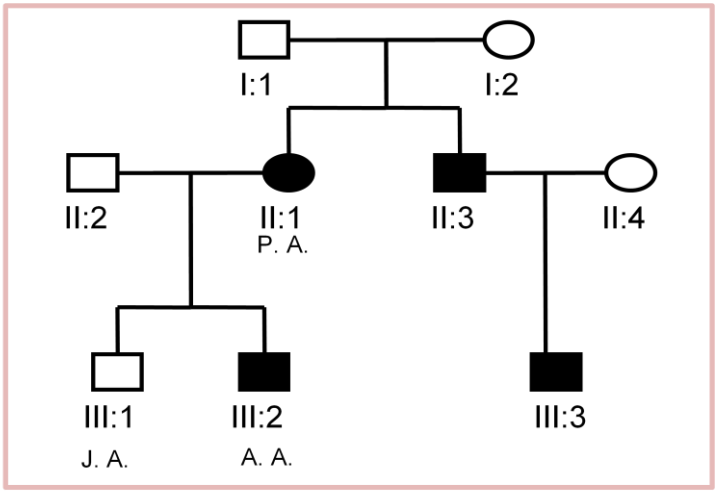

Fig. 1 - Family A.: no mutations in *BEST1.*

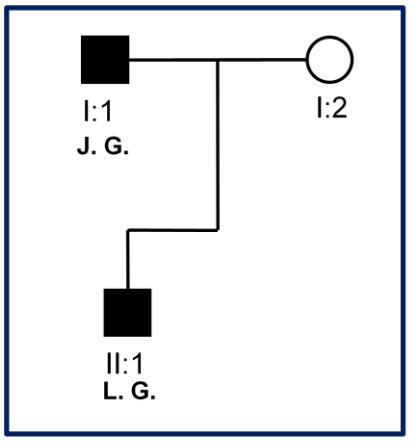

Fig. 2 - Family G.: no mutations in *BEST1*.

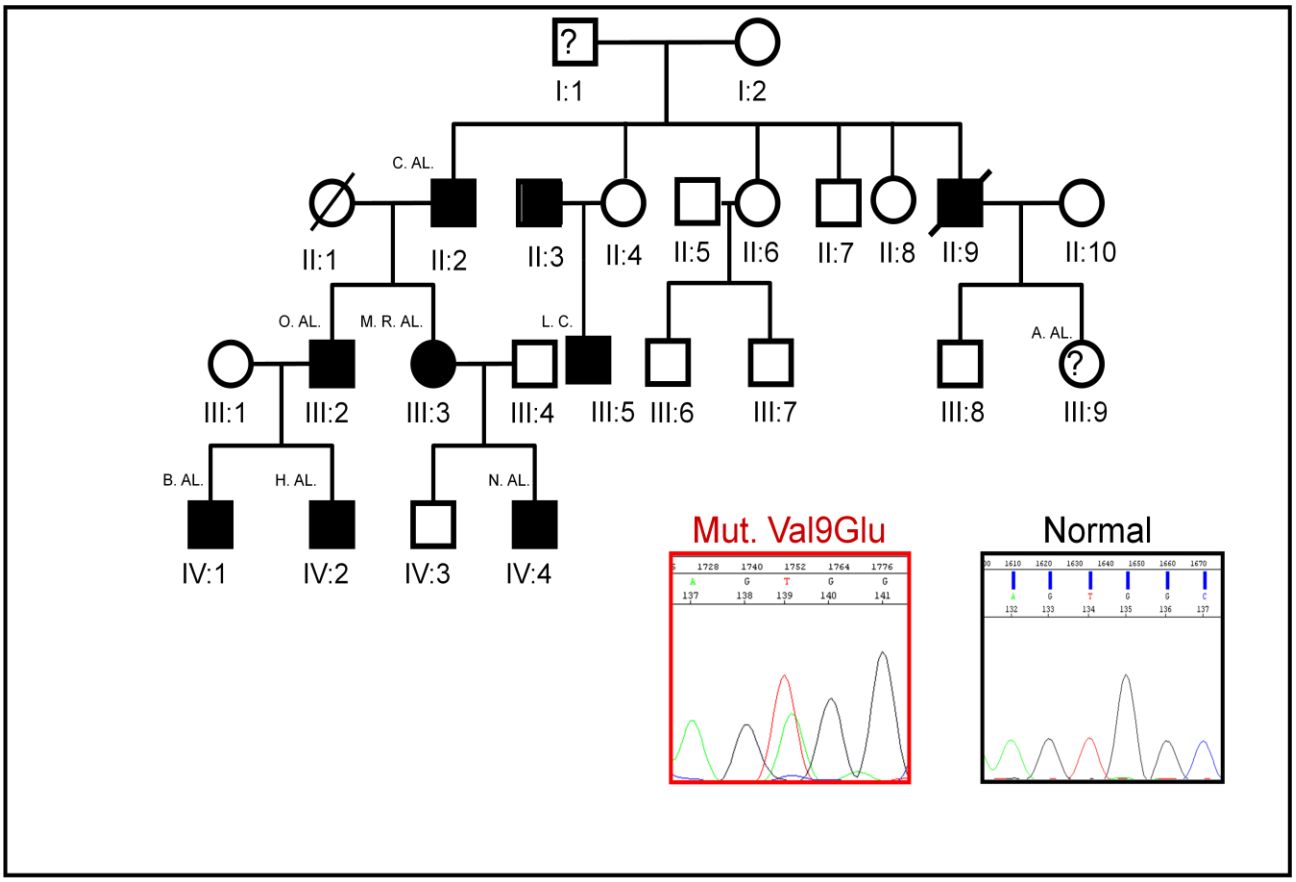

Fig. 3 - Family AL.: novel *BEST1* mutation Val9Glu.

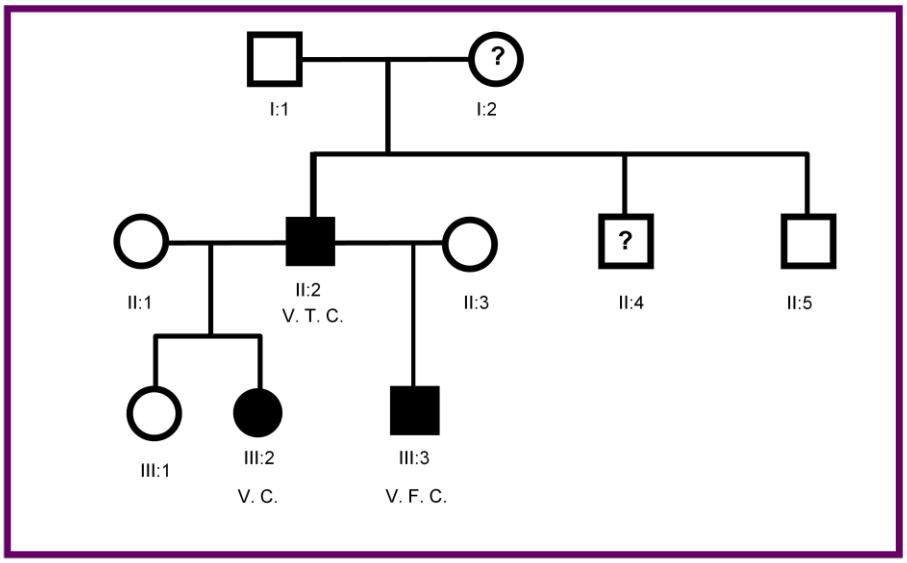

Fig. 4 - Family C.: novel *BEST1* mutation Leu234Val.

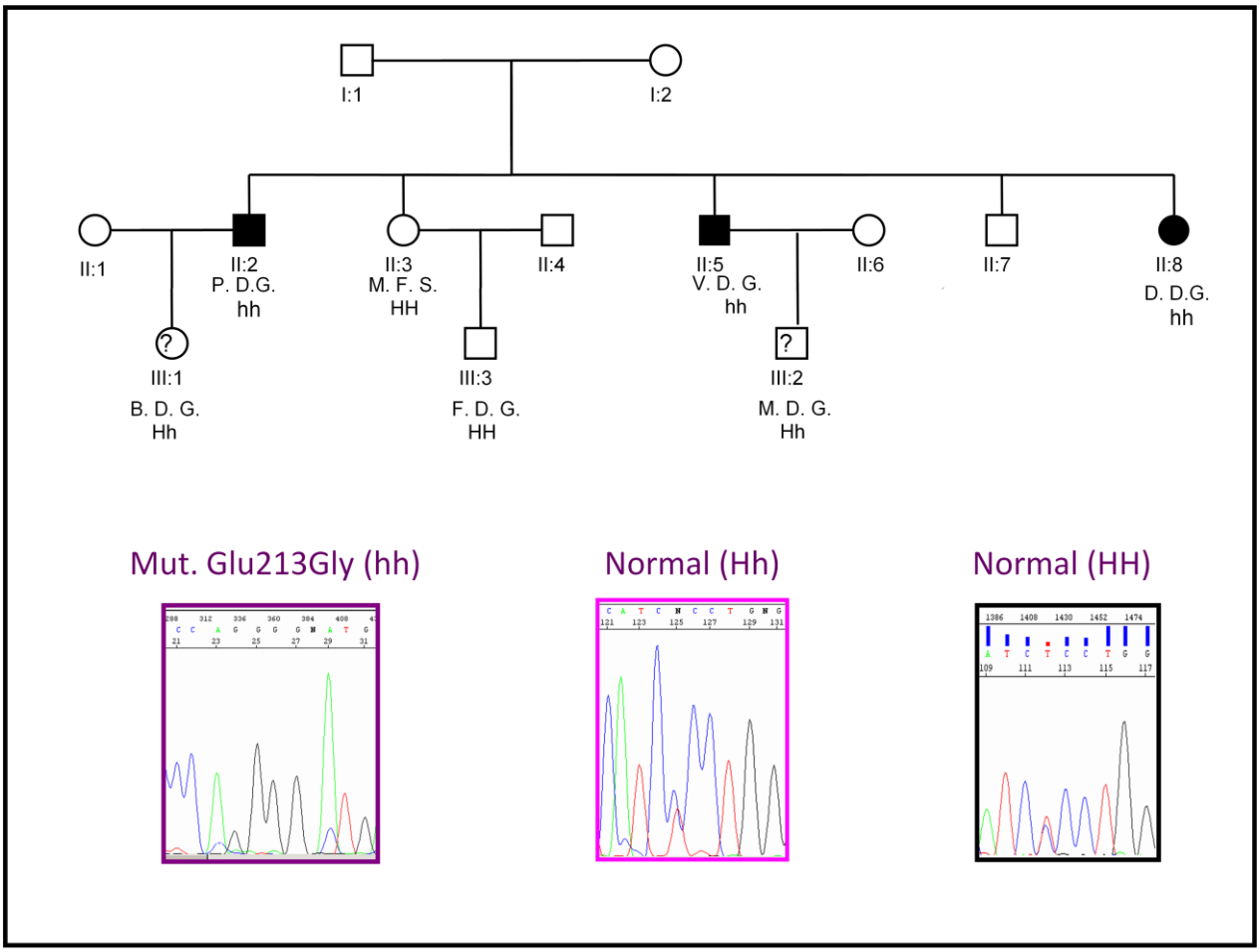

Fig. 5 - Family D.G.: novel *BEST1* mutation Glu213Gly

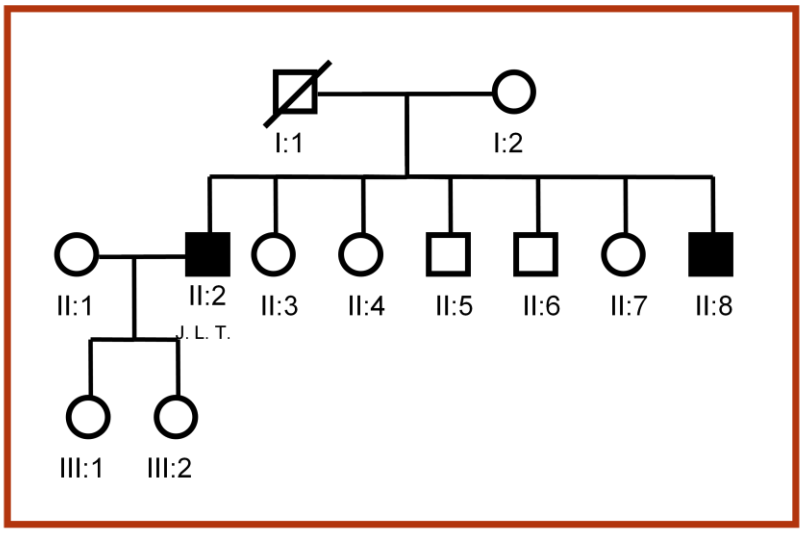

Fig. 6 - J.L.T.: no mutations found in *BEST1*.

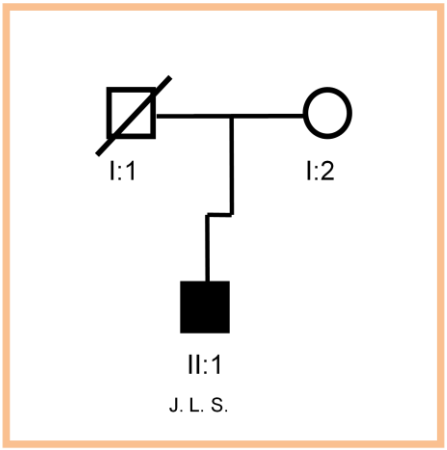

Fig. 7 - J.L.S.: no mutations found in *BEST1*.

Fig. 1 – 4: Representative pedigrees of patients with classic Best; **Fig. 5:** representative pedigree of a family with ARB; **Fig. 6 – 7:** Representative pedigrees of two independent patients with multifocal Best.

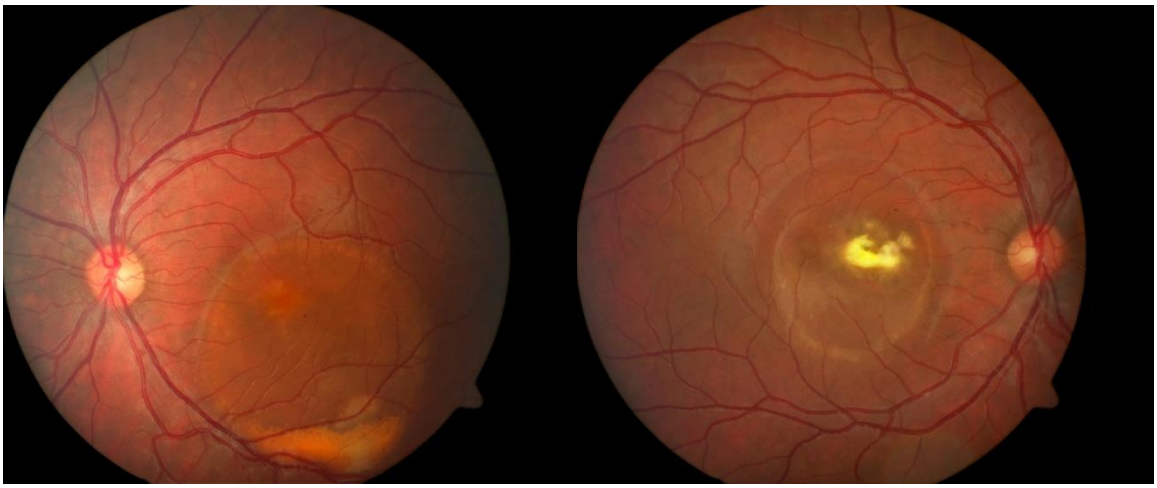

A - V.F.C. (male, Family C.)

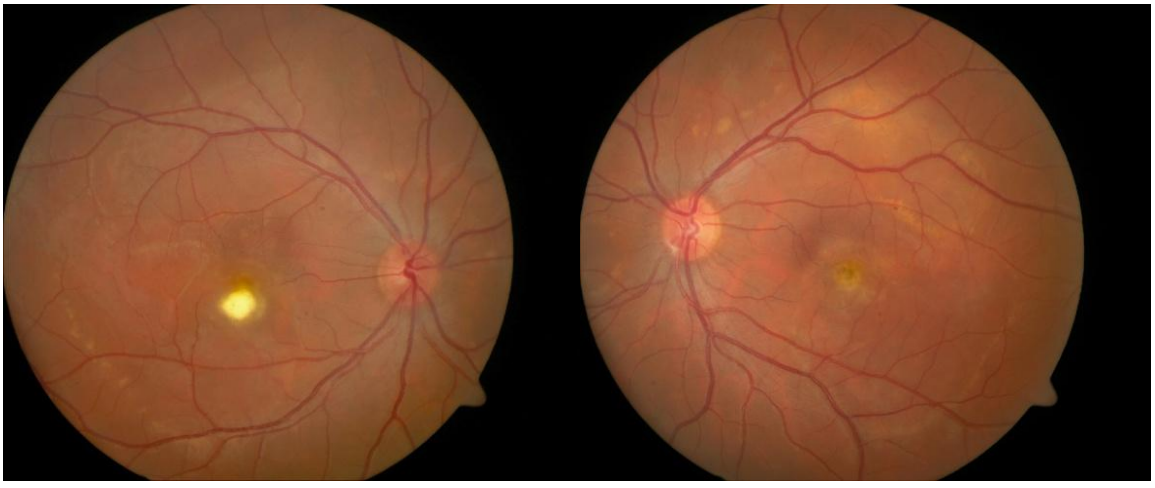

B - L.G. (male, Family G.)

Fig. 8 (A and **B)** – Best patients. Fundus photographs show: a well-demarcated, yellow and round lesion in both eyes (**A**); an egg-yolk lesion, evolving to an atrophic area inferior to fovea (OD) and a little atrophic area inferior to fovea (OS) (**B**).

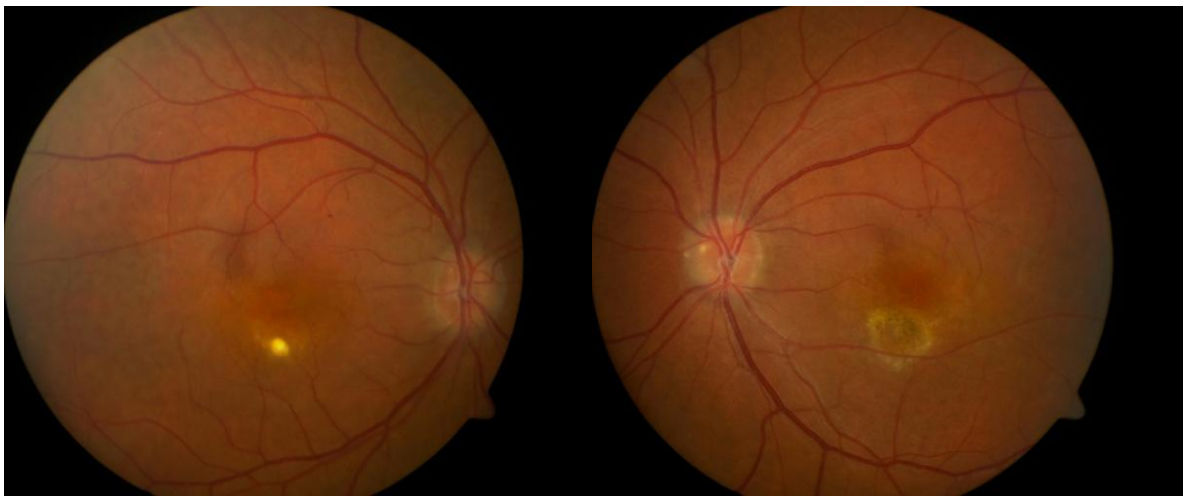

a - P.D.G. (male, Family D.G.)

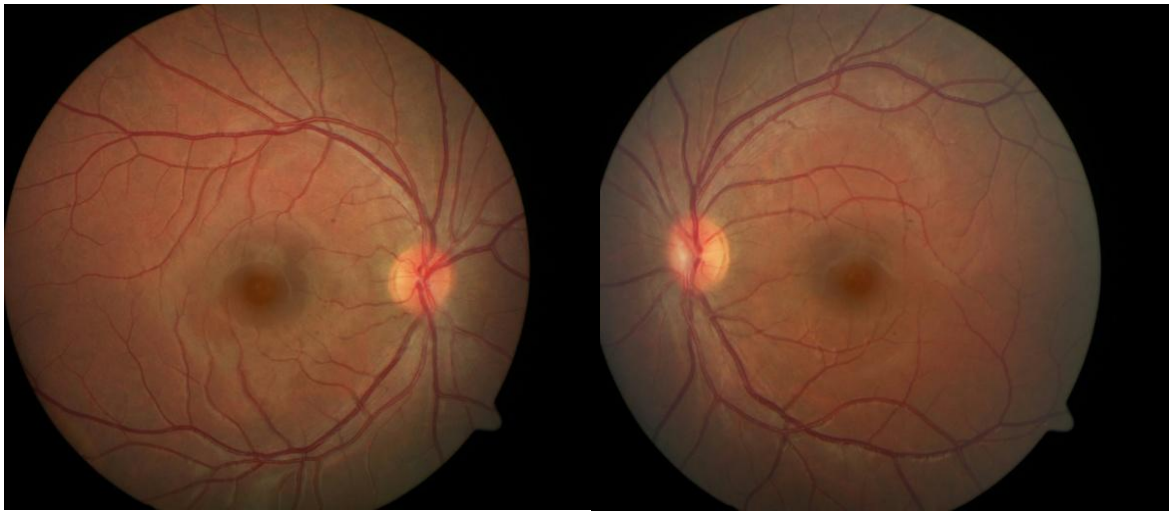

b - B.D.G. (female, Family D.G.)

Fig. 9 (a and **b)** – ARB patients. Fundus photographs show: a stage II lesion inferior to fovea (OD) and an atrophic lesion inferior to fovea (OS) (**a**); no significant changes (OU) (**b**).

We detected a novel amino acid change (Val9Glu) in *BEST1* gene in 7 patients from a Portuguese BVMD family (**Fig. 3** and **Table I**); this change was not present in either the tested unaffected family members or in the 102 chromosomes from healthy Portuguese controls. This novel T>A transversion at nucleotide 26 – V9E - replaces an amino acid residue for another of different nature - valine (nonpolar, neutral, hydropathy index (HI) of 4.2) for glutamic acid (polar, acidic and HI of 3.5). All BVMD patients with V9E mutation had an abnormal EOG, BCVA ranging from 2/10 to 10/10, variable macular degeneration ranging from mild stage I yellowish deposits to cicatricial changes that may be seen early in the disease process. Multifocal ERG was significantly altered in all affected family members, but did not correlate linearly with BCVA. For all affected members, the age of onset ranged from 5 to 15 years.

Another novel mutation found in exon 2 of *BEST1*: Glu35Lys (**Table I**) was detected in a single affected individual without prior family history of retinal disease. This novel substitution was not detected in 102 Portuguese healthy controls. The patient has an early disease onset (14 years), significantly reduced visual acuity, a decreased Arden ratio on EOG and an altered OCT.

Two novel missense mutations were found in exon 6 of *BEST1*: Glu213Gly and Leu234Val. The novel sequence change c.638A>G leading to the amino acid substitution Glu213Gly was found in homozygous state (hh) in three members of this ARB family but neither in their unaffected sister (**Fig. 5**, II:3) nor in 102 control chromosomes. Those patients (Family D.G.; **Fig. 5**), with no other causative sequence change, were severely affected, had an abnormal EOG and the onset of visual loss between 24 and 30 years. The son and daughter of two of them were confirmed to be carriers (Hh) and showed no sign of

macular degeneration by ophthalmological examination. However, the girl's EOG and mfERG were found to be subnormal, even in the absence of other clinical findings.

The novel missense mutation - Leu234Val - was segregated in a BVMD Portuguese family (Family C.) in which no other mutation in *BEST1* was found (**Fig. 4**). This novel substitution has not been detected in genomic DNA samples from 102 healthy controls of unrelated origin. Thus, Leu234Val is considered to be causative of BVMD.

Table I – Clinical data and mutations involved for the patients with Best disease presented in this study

Family Patient Sex	Age at onset (years)	Age at examination	DNA	Visual Acuity OD OS	Biom.	Fundus	EOG Arden-ratio OD/OS	mfERG	OCT
Family A (P.A.) female	NA	36	No mutations in *BEST1*	8/10 8/10	N	OU: central yellowish deposits stage I	1,42/1,53	Central dysfunction till ~15°, Max peaks: ~65nV/deg^2(OD) and 49nV/deg^2(OS)	**OCT**: OD → Z0=230/ Z1=233/ Z2=193 OS → Z0=235/ Z1=240/ Z2=197
Family A (A.A.) male	7	10	No mutations in *BEST1*	8/10 8/10	N	OD: yellow, round lesion with ~250 µm OS: N	1,31/ 1,04	Central dysfunction till ~15°, Max peaks: ~35nV/deg^2(OS) and 11nV/deg^2(OD)	**OCT**: OD → Z0=201/ Z1=260/ Z2=208 OS → Z0=198/ Z1=260/ Z2=210
Family G (J.G.) male	40	56	No mutations in *BEST1*	10/10 10/10	Pseudo-faquia OU	OD: N OS: cicatricial perifoveal lesion	1,69/ 1,23	Altered OU, Max peaks: 45nV/deg^2 decentered 10° (OD) and central peak of 38,1nV/deg^2 (OS)	**OCT**: OD → Z0=265/ Z1=294/ Z2=234 OS → Z0=307/ Z1=299,25/ Z2=242
Family G (L.G.) male	7	22	No mutations in *BEST1*	8/10 10/10	N	OD: egg-yolk lesion evolving to an atrophic area inferior to fovea OS: little atrophic area inferior to fovea	1,43/ 1,46	Altered OU, Max peaks: 51 nV/deg^2 decentered 10° (OD) and central peak of 55nV/deg^2(OS)	**OCT**: OD → Z0=335/ Z1=312,75/ Z2=289,25 OS → Z0=198/ Z1=260,5/ Z2=263,25
Family AL (O.AL.) male	5-15	35	Novel *BEST1* mutation Val9Glu	3/10 9/10	N	OD: scrambled egg/ atrophy in macula OS: atrophic central macular lesion	1,38/1,41	Altered OU, Max peaks: 21,1 nV/deg^2 (OD) and 23,6 nV/deg^2 (OS)	**OCT**: OD → Z0=147/ Z1=211/ Z2=240 OS → Z0=268/ Z1=229/ Z2=231

Table I – (continued)

Family AL (M.R.AL.) female	5-15	44	Novel *BEST1* mutation Val9Glu	4/10 3/10	N	OU: central atrophic macular lesions with pigmented changes	1,50/1,51	Altered OU, Max peaks: 22,4 nV/deg^2 (OD) and 31,3 nV/deg^2 (OS), decentered 10° 34,1 nV/deg^2 (OD)	NA
Family AL (L.C.) male	5-15	36	Novel *BEST1* mutation Val9Glu	5/10 5/10	N	OU: central lesions (3mm) with cicatricial changes	1,31/1,27	Altered OU, Max peaks: 28,8 nV/deg^2 (OD) and 27,4 nV/deg^2 (OS); 58 nV/deg^2 decentered 10° (OD)	**OCT**: OD → Z0=359/ Z1=347/ Z2=251 OS → Z0=466/ Z1=418/ Z2=241
Family AL (A.S.AL.) female	5-15	25	Novel *BEST1* mutation Val9Glu	8/10 8/10	N	OU: central yellowish deposits stage I	1,53/1,46	Altered OU, Max peaks: 66,4 nV/deg^2 (OD) and 79,1 nV/deg^2 (OS)	NA
Family AL (B.AL.) male	5-15	24	Novel *BEST1* mutation Val9Glu	5/10 5/10	N	OU: central lesions with atrophic areas and scarring	1,39/1,43	Altered OU, Max peaks: 26,7 nV/deg^2 (OD) and 33,3 nV/deg^2 (OS)	**OCT**: OD → Z0=300/ Z1=302/ Z2=222 OS → Z0=351/ Z1=356/ Z2=210
Family AL (H.AL.) male	7	14	Novel *BEST1* mutation Val9Glu	10/10 2/10	N	OD: central egg-yolk lesion (2mm) OS: scrambled egg and atrophic scarring	1,52/1,46	Altered OU, Max peaks: 31,1 nV/deg^2 and 29,5nV/deg^2 decentered 10° (OU)	**OCT**: OD → Z0=306/ Z1=267/ Z2=227 OS → Z0=227/ Z1=216/ Z2=220
Family AL (N.AL.) male	8	19	Novel *BEST1* mutation Val9Glu	10/10 10/10	N	OU: central yellowish deposits stage I	2,51/0	Altered OU, Max peaks: 36,4 nV/deg^2 (OD) and 26,0 nV/deg^2 (OS)	**OCT**: OD → Z0=324/ Z1=264/ Z2=244 OS → Z0=180/ Z1=241/ Z2=238

Table I – (continued)

Family C (V.T.C.) Male	NA	53	Novel *BEST1* mutation Leu234Val	2/10 7/10	N	OU: pigmented fibrous scarring of macular areas. Yellowish deposits and atrophy.	1,15/1,17	Altered OU, Max peaks: 46,6 nV/deg^2 (OD) and 60,8 nV/deg^2 (OS)	**OCT**: OD → Z0=280/ Z1=278/ Z2=233 OS → Z0=143/ Z1=240/ Z2=195
Family C (V.C.) Female	12	25	Novel *BEST1* mutation Leu234Val	8/10 8/10	N	OU: central stationary scrambled egg lesions (1,5 mm)	1,09/1,27	Altered OU, Max peaks: 88,4 nV/deg^2 (OD) and 60,8 nV/deg^2 (OS)	**OCT**: OD → Z0=346/ Z1=294/ Z2=264 OS → Z0=215/ Z1=292/ Z2=270
Family C (V.F.C.) male	7	16	Novel *BEST1* mutation Leu234Val	2,5/10 10/10	N	OU: stage III stationary, scrambled egg lesion and macular scar	1,01/1,02	Altered OU, Max peaks: 96,3 nV/deg^2 (OD) and 60,2 nV/deg^2 (OS)	**OCT**: OD → Z0=355/ Z1=351/ Z2=258 OS → Z0=465/ Z1=408/ Z2=341
M.J.A. female	41	59	No mutations in BEST1	1/10 1/10	N	OU: macular hyper pigmentation affecting fovea	1,19/0,93	NA	NA
S.V.M. female	14	15	Novel *BEST1* mutation Glu35Lys	4/10 < 1/10	N	OD: ¾ DD centro-macular egg yolk (stage II) OS: cicatricial lesion affecting fovea	1,39/1,41	NA	**OCT**: OD → Z0=374/ Z1=310/ Z2=258 OS → Z0=230/ Z1=280/ Z2=253
A.R.N.R. male	42	50	Pending	3/10 3/10	OU: Incipient cataract	OU: scrambled egg inferior to macula	1,50/1,42	NA	**OCT**: OD → Z0=345/ Z1=304/ Z2=264 OS → Z0=315/ Z1=292/ Z2=270

Table II – Clinical data and mutations involved for the patients with ARB presented in this study

Family Patient Sex	Age at onset (years)	Age at examination	DNA	Visual Acuity OD	Visual Acuity OS	Biom.	Fundus	EOG Arden-ratio OD/OS	mfERG	OCT
Family DG (P.D.G.) male	29	41	Novel *BEST1* mutation Glu213Gly (hh)	10/10	2/10	N	OD: stage II inferior to fovea OS: atrophic lesion inferior to fovea; disc drusen	1,20/1,00	Altered OU, Max peaks: 21,0 nV/deg^2 (OD) and 17,4 nV/deg^2 (OS)	**OCT**: OD → Z0=233/ Z1=249/ Z2=219 OS → Z0=229/ Z1=242/ Z2=214
Family DG (V.D.G.) male	30	40	Novel *BEST1* mutation Glu213Gly (hh)	2/10	2/10	N	OU: scrambled egg lesion perifoveal	1,08/1,08	Altered OU, Max peaks: 16,8 nV/deg^2 (OD) and 31,7 nV/deg^2 (OS)	NA
Family DG (D.M.G.) Female	24	24	Novel *BEST1* mutation Glu213Gly (hh)	10/10	7/10	N	OD: multiple flecks rounding fovea; orange pigmented foveal lesion OS: infra-foveal lesion (sub-retinian fibrosis) + orange pigmented lesion	2,65/1,45	NA	NA
Family DG (B.G.) Female	8	13	Novel *BEST1* mutation Glu213Gly (Hh)	6/10	6/10	N	OU: with no significant alterations	1,49/1,61	Altered OU, Max peaks: 75,7 nV/deg^2 (OD) and 85,4 nV/deg^2 (OS)	**OCT**: OD → Z0=199/ Z1=277/ Z2=239 OS → Z0=180/ Z1=277/ Z2=236
Family Alm. (J.E.A.) male	28	32	Pending	3/10	4/10	OD: mild subcapsular lens opacification OS: N	OU: yellowish centromacular deposits	1,25/1,16	Altered OU, Max peaks: 36,3 nV/deg^2 (OD) and 13 nV/deg^2 (OS)	**OCT**: OD → Z0=294/ Z1=365/ Z2=398 OS → Z0=341/ Z1=403/ Z2=406

Table III – Clinical data and mutations involved for the patients with multifocal Best presented in this study

Family Patient Sex	Age at onset (years)	Age at examination	DNA	Visual Acuity OD	Visual Acuity OS	Biom.	Fundus	EOG Arden-ratio OD/OS	mfERG	OCT
Family T. (J.L.T.) male	50	57	No mutations in *BEST1*	1/10	6/10	OD: N OS: subcapsular posterior cataract	OD: hipopigmented atrophic macular area OS: dispersed egg yolk lesions	1,73/1,84 (both border-line)	Altered OU, Max peaks: 32,3nV/deg2 (OD) e 35,3nV/deg^2 (OS)	**OCT**: OD → Z0=182/ Z1=270/ Z2=243 OS → Z0=193/ Z1=290/ Z2=249
Family S. (J.L.S.) male	33	46	Pending	10/10	10/10	N	OU: yellowish extra-fovea lesions of multifocal Best	1,13/1,34	Altered OU, Max peaks: ~65,4nV/deg^2 (OD) e 76,3nV/deg^2 (OS)	**OCT**: OD → Z0=218/ Z1=283/ Z2=244 OS → Z0=221/ Z1=283/ Z2=241

OD – right eye; OS – left eye; OU – both eyes; Biom. – Biomicroscopy; EOG – Electro-oculogram; mfERG – multifocal Electroretinogram; OCT – Optical Coherence Tomography; N – normal; NA – not available; stage I – pre-viteliform stage; stage II – vitelliform stage; stage III – pseudohypopyon stage.

Electrophysiological findings

Typical EOG findings, with a reduction in the EOG light rise, were shown in most patients. In the BVMD sub-group we found reduced Arden ratios in all families However, these values were extremely reduced in family C, within the range normally found for the ARB phenotype (Burgess et al, 2008). Family D.G., with a confirmed molecular diagnosis compatible with ARB also showed Arden ratio values well below the limits, compared with most BVMD families (**Table I and II**).

In all affected individuals, clinical electrophysiology demonstrated abnormal multifocal ERGs. There was a substantial reduction in mfERG amplitude responses in BVMD patients when compared with controls (**Fig. 10** and **11** for both N1 and P1 components). With regard to the N1 and P1 mfERG components, amplitudes were found to be dramatically reduced for all rings in BVMD patients. Maximum peaks in mfERG responses ranged from a minimum value of 11 nV/deg^2 (recorded in the left eye of the youngest affected member of family A) to 96,3 nV/deg^2 (recorded in the right eye of the youngest member of family C). Intrafamilial heterogeneity is observed, especially in family AL, where amplitude reduction of maximum peaks does not seem to be age-dependent. Abnormal mfERG responses were found for all tested eccentricities, though effect size was clearly smaller for more peripheral rings.

In the ARB sub-group of patients, maximum peaks on mfERG ranged from a minimum of 16,8 nV/deg2 and 31,7 nV/deg2; it should be underscored that the heterozygous carrier (Figure5, III-1) also revealed subnormal peaks ranging from 75,7 nV/deg2 and 85,4 nV/deg2 with no eccentricity.

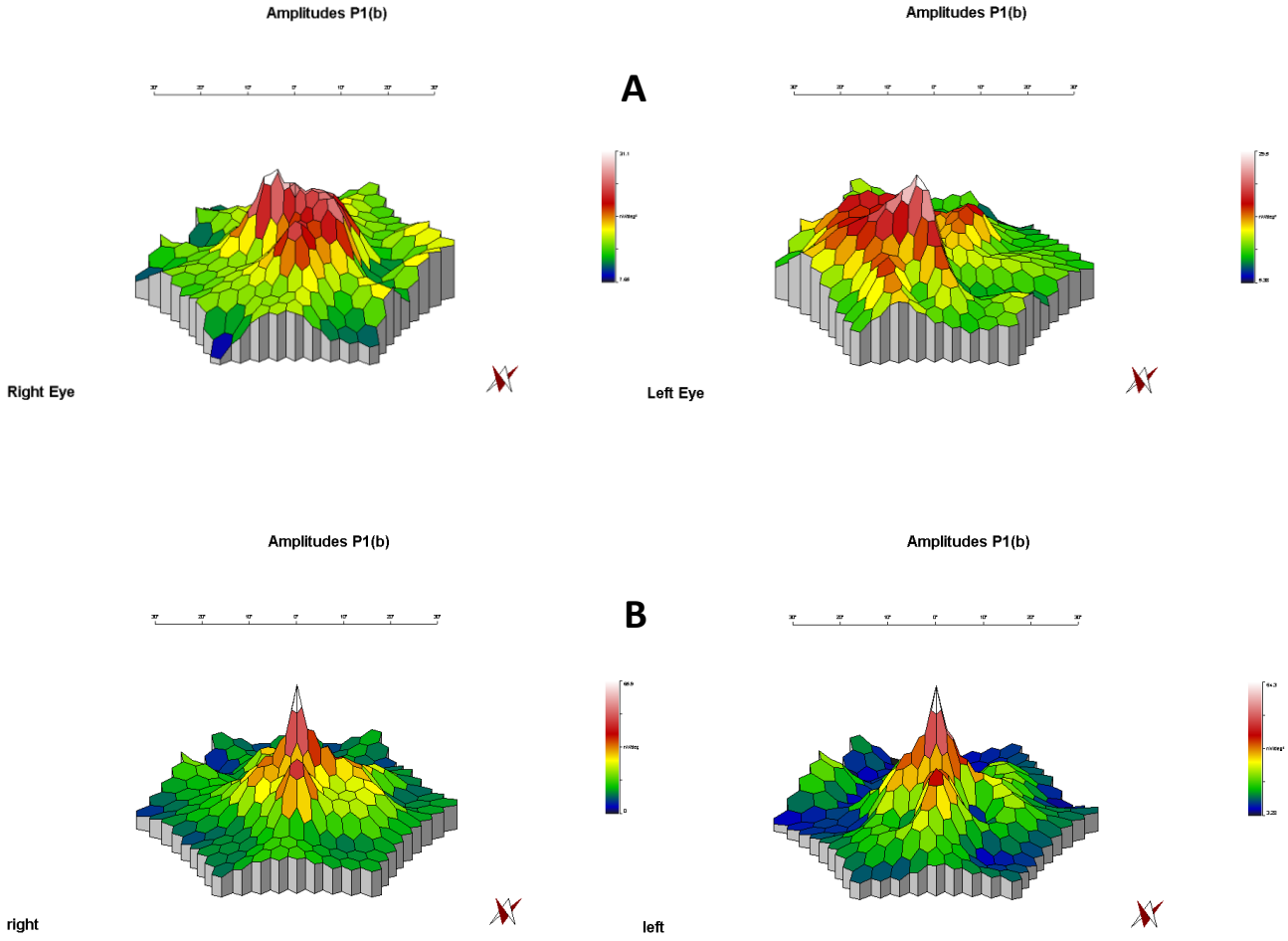

Fig. 10 – mfERG recordings in BVMD patients (see **Table I** for recorded data). **A:** patient H. AL. with a central egg-yolk lesion (OD) and scrambled egg and atrophic scarring (OS). **B:** J.G. with later age at onset, normal OD and a cicatricial perifoveal lesion (OS).

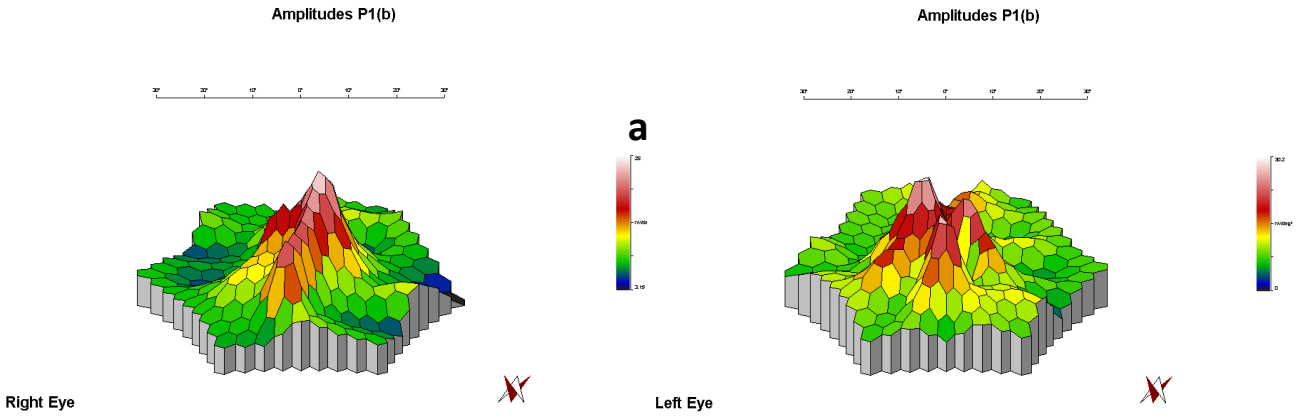

Fig. 11 – mfERG recordings in an ARB patient (see **Table II** for recorded data). **a:** patient P.D.G. with a lesion in stage II (OD) and an atrophic lesion (OS) inferior to fovea.

For the 2 patients with multifocal Best disease, peak amplitudes were below normal; however, since only 2 isolated cases were analyzed the differences observed may represent the normal course of disease.

OCT findings

Representative images from OCT imaging are shown in **Figure 12, 13** and **14.** OCT images acquired through the fovea showed heterogeneity, from preserved central foveal depression and mild thickness increase of the retina to loss of central foveal depression, detachment of RPE and substantial thickness increase of the retina. OCT showed a hyporreflective structure beneath retina and RPE that is compatible with the lipofuscin material. Consequently, the superficial layers of the retina appeared thinned and severely altered. Thickness values for Z0 correlated well with the fundus images and disease stages, for all patients in the 3 sub-groups. However, no correlation was observed between OCT central thickness and BCVA; usually very low BCVA values are seen in more severely affected individuals that present central macular atrophic/scarring lesions with near normal thickness on OCT but disorganized structure.

None of the affected individuals of our cohort displayed changes compatible with choroidal neovascularization on OCT imaging.

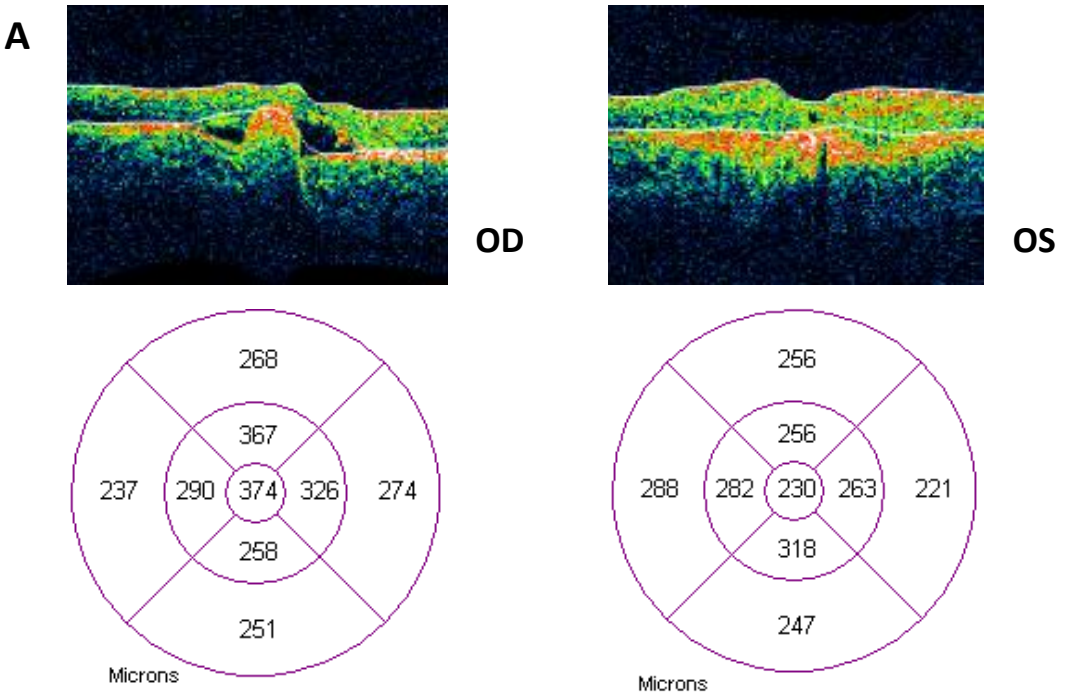

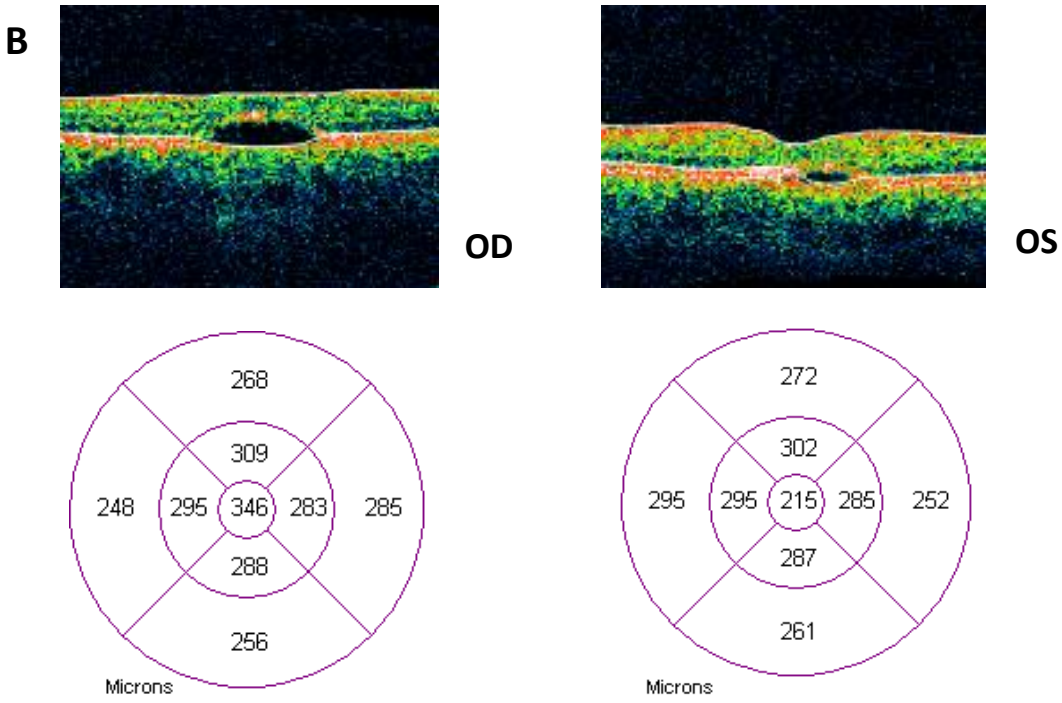

Fig. 12 – OCT recordings in BVMD patients (see **Table I** for recorded data). **A:** patient S.V.M. with loss of central foveal depression and substantial increased thickness of the retina (OU). **B:** V.C. with loss of central foveal depression and substantial increased thickness of the retina.

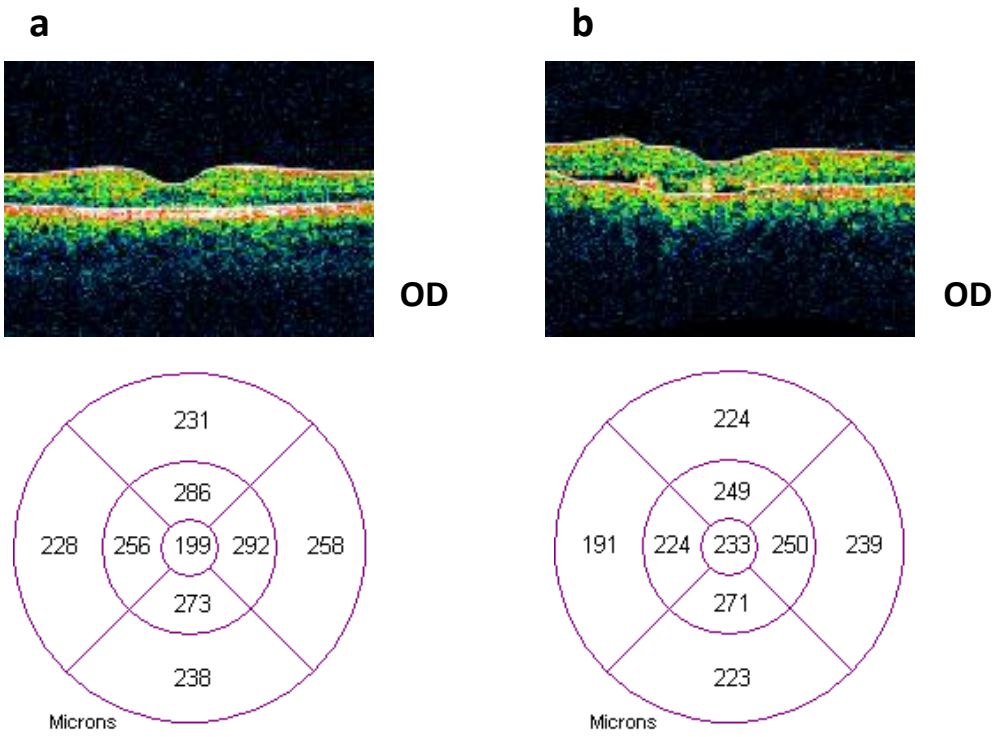

Fig. 13 – OCT recordings in ARB patients (see **Table II** for recorded data). **a:** patient B.D.G. (**Fig. 5** – III:1) near normal total retinal thickness for all rings; the RPE layer is thicker across this section (heterozygous carrier) **b:** P.D.G (**Fig. 5** – II:2) significant disorganization of all retinal layers, with cystic formations above and within the RPE layer in an homozygous affected ARB patient.

Discussion

Best Disease is known to have variable penetrance and expressivity. In the present study this heterogeneity is observed even in patients within the same family. Many patients maintain a good visual acuity for decades, which may lead to later diagnosis of the disease. In fact, the diagnosis of many variants of the BEST1 related clinical continuum, especially the milder forms may be diagnosed as part of a routine "normal" eye exam. In Family C. (**Table I**) was identified a novel *BEST1* mutation Leu234Val, with autosomal dominant inheritance (**Fig. 4**). The affected members of this family show an extremely low EOG (Arden ratio between 1,01 and 1,27), moderate alterations in mfERG and fundus photography with advanced stage lesions early in life. However, their VA is generally preserved. The apparent low vision of the right eye (patient VFC) seems to be a consequence of uncorrected refractive amblyopia, unrelated with BVMD. The vision loss observed in the older individual of this family simply reflects the normal course of disease.

Late-onset symptoms are not uncommon and these individuals with *BEST1* mutations, even if they already have electrophysiologic and morphologic alterations, could be undiagnosed or later diagnosed. In some cases, the decrease of VA with the duration of the disease may be due to environmental or genetic factors. These modifiers can be another explanation for the decreased penetrance and variable expressivity in *BEST1* associated phenotypes (Boon et al., 2009).

In this paper we also study families with autosomal recessive bestrophinopathy, like family DG and another isolated case with unknown family history. Family DG was previously defined as a Best-like case, with autosomal-dominant ocular phenotypes. The affected

members of this family show vitelliform lesions characteristic of Best disease on fundus photography, contrary to Burgess' conclusions (Burgess et al., 2008). They also have low Arden ratios on EOG and considerable alterations on mfERG. Molecular findings revealed a novel *BEST1* mutation Glu213Gly in homozygous state in three patients of family DG and in heterozygous state in two cousins (**Fig. 5 –** III:1 and III:2). It should be underscored that this is the first Portuguese family described with this phenotype and confirmed from a molecular standpoint. The homozygote patients show an extremely low Arden ratio and also abnormalities on mfERG. Their visual acuity seems to be related with lower EOG. The heterozygote boy was confirmed to be carrier but he had no sign of disease. On the other hand, the heterozygote girl (B.D.G., **Fig. 5 –** III:1 and **Table II**) had an abnormal EOG (Arden ratio 1,49 OD; 1,61 OS), altered mfERG and a mild thickness increase of the retina (central foveal depression was preserved). This findings contrast with the fundus photography that showed no significant alterations. Consanguinity is highly probable since both sides of the family originate from a small isolated village.

Our results indicate that a strict classification in stages is too rigid, because many of the BVMD lesions show aspects of different stages (Boon et al., 2009). Most BVMD lesions remain stationary after a considerable follow-up period, but our study also illustrates that a minority of lesions may show notable stage changes within less than a year.

The present study provides new insights into structure-function correlations at the level of the neurosensory retina in BVMD, including the involvement of the central and peripheral cone pathways, and their relationship with clinical markers of disease progression. Accordingly, our work confirmed that BMD patients have neurosensory retina dysfunction up to 30°, as shown by reduced mfERG peak amplitudes. This functional

impairment, which, according to Hood (Hood, 2000) can be speculated to be attributed to either cone photoreceptor cell loss or damage to the cone outer segments (Scholl, et al., 2002; Schatz, et al., 2006; Glybina, et al., 2006). There is a pan-retinal defect in BVMD corroborated by the recently reported abundant expression of (mutated) bestrophin in the peripheral retina and of global retinal pigment epithelial failure (as obtained by the commonly altered EOG measures) (O'Gorman, et al., 1988; Maloney, et al., 1977; Mullins, et al., 2007; Marmor, et al., 1993; Seddon, et al., 2003). We believe that the extension of retinal damage and the familial intravariability and intervariability of age of onset and range of visual loss are part of a scenario of variable expression in BVMD.

In our study there is no reference of choroidal neovascularization, which allow us to conclude that it is rare in this type of retinal dystrophy, in agreement with other findings in the literature.

In conclusion, the definitive diagnosis of Best Vitelliform Macular Dystrophy and Autosomal Recessive Bestrophinopathy are best based on molecular genetics. Phenotypical analysis is essential to identify the role of RPE functional changes in the determination of the clinical diagnosis. Genotype-phenotype correlations allow us to better understand the pathophysiology of RPE related diseases.

Agradecimentos

Gostaria de agradecer a todos os doentes e às suas famílias pela participação no estudo realizado. Ao meu orientador Prof. Doutor Eduardo José Gil Duarte Silva um agradecimento especial pela oportunidade em realizar este trabalho, pela atenção e apoio disponibilizados e pelos conhecimentos e experiência transmitidos. Um agradecimento também a todos os que colaboraram neste estudo, pela disponibilização de dados e imagens, que permitiram a concretização deste trabalho.

References

Boon, C.J F., Theelen, T., Hoefsloot, E.H., et al. (2009). Clinical and Molecular Genetic Analysis of Best Vitelliform Macular Dystrophy. J Retina Vitr Dis 29: 835-847.

Boon, C.J.F., den Hollander, A.I., Hoyng, C.B., et al. (2009). The spectrum of ocular phenotypes caused by mutations in the BEST1 gene. Prog Retinal Eye Res 28: 187-205.

Boon, C.J.F., Klevering, B.J., Keunen, J.E.E., et al. (2008). Fundus autofluorescence imaging of retinal dystrophies. Vis Res 48: 2569-2577.

Burgess, R., Millar, I.D., Leroy, B.P. et al. (2008). Biallelic mutation of BEST1 causes a distinct retinopathy in humans. Am J Hum Genet, 82: 19-31.

Furino, C. et al. (2008). Fundus autofluorescence, Optical Coherence Tomography and Visual Acuity in Adult-Onset Foveomolecular Dystrophy. Ophthalmologica , 222: 240-244.

Glybina, I.V., Frank, R.N. (2006). Localization of multifocal electroretinogram abnormalities to the lesion site: findings in a family with Best disease. Arch Ophthalmol, 124: 1593-1600.

Hayami, M., Decock, C.H.R., Brabant, P., et al. (2003). Optical Coherence Tomography of Adult-Onset Vitelliform Dystrophy. Bull Soc Belge Ophtalmol, 289: 53-61.

Hood, D. S. (1997). A comparison of the components of the multifocal and full-field ERGs. Vis Neurosci, 14: 533-544.

Hood, D.C. (2000). Assessing retinal function with the multifocal technique. Prog Retinal Eye Res, 19: 607-646.

Kutschbach, E. (1997). Method for Multifocal ERG Using Short Length and Corrected M-Sequences. Wiesbaden: Roland Consult Elektrophysiologische Diagnostik Systeme .

Maloney, W.F., Robertson, D.M., Duboff, S.M. (1977). Hereditary vitelliform macular degeneration: variable findings within a single pedigree. Arch Ophthalmol, 95: 979-983.

Marmor, M.F., Zrenner, E. (1993). Standard for clinical electro-oculography. Doc Ophthalmol 85, 115-124.

Marmorstein, A. D. et al. (2009). Functional roles of bestrophins in ocular epithelia. Prog Retina Eye Res , 28, pp. 206-226.

Marquardt, A., Stöhr, H., Passmore, L.A., et al. (1998). Mutations in a novel gene, BEST1, encoding a protein of unknown properties cause juvenile-onset vitelliform macular dystrophy (Best's disease). Hum Mol Genet, 7: 1517-1525.

Mullins, R.F., Kuehn, M.H., Faidley, E.A., et al. (2007). Differential macular and peripheral expression of bestrophin in human eyes and its implication for Best disease. Invest Ophthalmol Vis Sci. , 48, pp. 3372-3380.

O'Gorman, S., Flaherty, W.A., Fishman, G.A., et al. (1988). Histopathologic findings in Best's viteliform macular dystrophy. Arch Ophthalmol , 106, pp. 1261-1268.

Petrukhin, K., Koisti, M.J., Bakall, B., et al. (1998). Identification of the gene responsible for Best macular dystrophy. Nat Genet , 19, pp. 241-247.

Pierro, L., Tremolada, G., Introini, U., et al. (2002). Optical Coherence tomography findings in adult-onset macular dystrophy. Am J Ophthalmol. , 134, pp. 675-680.

Querques, G., Bux, A.V., Prato, R., et al. (2008). Correlation of Visual Function Impairment and Optical Coherence Tomography Findings in Patients with Adult-Onset Foveomacular Vitelliform Macular Dystrophy. Am J Ophthalmol , 146, pp. 135-142.

Querques, G., Regenbogen, M., Quijano, C., et al. (2008). High-Definition Optical Coherence Tomography Features in Vitelliform Macular Dystrophy. Am J Ophthalmol , 146, pp. 501-507.

Saito, W., Yamamoto, S., Hayashi, M., et al. (2003). Morphological and functional analyses of adult onset vitelliform macular dystrophy. Br J Ophthalmol. , 87, pp. 758-762.

Schatz, P., Klar, J., Andreasson, S., et al. (2006). Variant phenotype of Best vitelliform macular dystrophy associated with compound heterozygous mutations in VMD2. Ophthalmic Genet. , 27, pp. 51-56.

Scholl, H.P., Schuster, A.M., Vonthein, R., et al. (2002). Mapping of retinal function in Best macular dystrophy using multifocal electroretinography. Vis Res , 42, pp. 1053-1061.

Seddon, J.M., Sharma, S., Chong, S., et al. (2003). Phenotype and genotype correlations in two Best families. Ophthalmology , 110, pp. 1724-1731.

Sun H., Tsunenari, T., Yau, K.W., et al. (2002). The vitelliform macular dystrophy protein defines a new family of chloride channels. Proc Natl Acad Sci USA , 99, pp. 4008-4013.

Wabbels, B., Preising, M.N., Kretschmann, U., et al. (2006). Genotype-phenotype correlation and longitudinal course in ten families with Best vitelliform macular dystrophy. Graefe's Arch Clin Exp Ophthalmol , 244, pp. 1453-1466.

White, K., Marquardt, A., Weber, B.H., et al. (2000). VMD2 Mutations in Vitelliform Macular Dystrophy (Best Disease) and Other Maculopathies. Human Mutat , 15, pp. 301-308.